Chiral Metal–Organic Cluster Induced High Circularly Polarized Luminescence of Metal–Organic Framework Thin Film

Yi-Hong Xiao, Peter Weidler, Shi-Sheng Lin, Christof Wöll, Zhi-Gang Gu, and Jian Zhang**

Guest-induced host–guest assembly in metal–organic frameworks (MOFs) has become a critical strategy to achieve circularly polarized luminescence (CPL). Herein, chiral metal–organic clusters (MOCs) induced CPL of achiral MOF are reported. Enantiopure titanium-oxo clusters (R/S-TOCs) are effectively loaded into the pores of a fluorescent, highly stable MOF NU-901 thin film by using a liquid-phase epitaxial layer-by-layer encapsulation method. The resulting chiral TOCs@NU-901 MOF thin films exhibit strong chirality, intense photoluminescence, and excellent CPL performance with the highest dissymmetry factor (±0.025) reported so far for the downshifted MOF-based materials. Further, the comparison experiments and density functional theory (DFT) calculations demonstrate that the excellent performance benefited from the strong chirality and charge transfer caused by the significant π–π interactions between the host (MOF) and guest (R/S-TOCs). This novel chiral MOCs induced approach provides a powerful toolbox for new host–guest CPL thin film materials.

1. Introduction

The development of circularly polarized luminescence (CPL) materials is driven by the demand from numerous application fields, e.g., photoelectric devices, 3D optical displays, information storages, and biological probes.[1] Conventional synthesis strategies for CPL materials involve the combination of chiral centers and achiral fluorophores to yield polymers,[2] self-assembled supramolecules,[3] metal complexes,[4] and metal–organic hybrid materials.[5] Among crystalline inorganic–organic hybrid materials, metal–organic frameworks (MOFs),[6] also referred to as porous coordination polymers (PCPs), are composed of metal ions (clusters) and organic ligands, recently attracting great attention in CPL due to their tunable structures and chiral optical properties.[7] However, such chiral optical MOFs (such as AIEgen MOF,[7a] chiral ZIFs,[7b] topological eta MOFs,[7c] $[Ln_2(\mu_4\text{-tar})_2(\mu\text{-tar})(H_2O)_2]\cdot xH_2O$,[7d] and $Zn_2(D/LCam)_2DAP$[7e]) materials simultaneously possessing chiral and luminescent functions not only undergo cumbersome synthesis procedures but hard to achieve high CPL performance. In addition, the dense fluorophores solid materials are prone to aggregation, which results in unwanted quenching effects reducing the efficiency of circularly polarized light generation.[8]

Thanks to the ordered nanopore systems of MOFs, they have widely served as ideal host matrices to load guest species for enhancing their properties and endowing new functionalities.[9] Recently, guest-induced host–guest assembly strategy[10] has been demonstrated to overcome some of the above-mentioned problems in the CPL MOFs-based materials.[8a,11] For example, chiral MOFs such as chiral ZIF-8,[8a] $Zn(l/d\text{-}l_{Cl})(Cl)](H_2O)_2$,[11a] γCD-MOF,[11c] and $[Zn_2(D/Lcam)_2dabco]_n$[11h] have been used as parent matrix to load guest species, yielding guest-induced CPL MOFs materials. However, the finite chiral MOFs as the host are yet unable to meet the long-term development of their CPL applications. The use of achiral MOFs as the host for loading chiral guests will greatly expand the MOFs-based CPL species, but so far such report is very scarce.[11g] Besides, the CPL performances of the reported MOF-based materials are still at a relatively low level (Table S1, Supporting information), which greatly limits their potential optical applications. Based on the above considerations, developing new chiral guests-induced achiral MOF-based materials to achieve high CPL performance is an extremely urgent task.

Discrete (0-D) metal–organic clusters (MOCs) with polynuclear metal-oxo clusters and tunable functional ligands exhibit unique physicochemical properties, which can serve as ideal dispersed guest candidates.[12] Particularly, nanosized MOCs with specific configurations such as chiral conjugated systems and chemical stability could be considered guests to be loaded into the pores of MOFs for expanding their functionalities. Here, we report the first example of chiral MOCs induced MOF-based CPL thin film and the approach that starts from an achiral, luminescent MOF, which then loads with suitable chiral MOCs to yield a record CPL.

Y.-H. Xiao, S.-S. Lin, Z.-G. Gu, J. Zhang
State Key Laboratory of Structural Chemistry
Fujian Institute of Research on the Structure of Matter
Chinese Academy of Sciences
Fuzhou 350002, P. R. China
E-mail: zggu@fjirsm.ac.cn; zhj@fjirsm.ac.cn
Y.-H. Xiao, Z.-G. Gu, J. Zhang
University of Chinese Academy of Sciences
Beijing 100049, P. R. China
P. Weidler, C. Wöll
Institute of Functional Interfaces (IFG)
Karlsruhe Institute of Technology (KIT)
76344 Eggenstein-Leopoldshafen, Germany
Z.-G. Gu, J. Zhang
Fujian Science & Technology Innovation Laboratory for Optoelectronic Information of China
Fuzhou, Fujian 350108, P. R. China

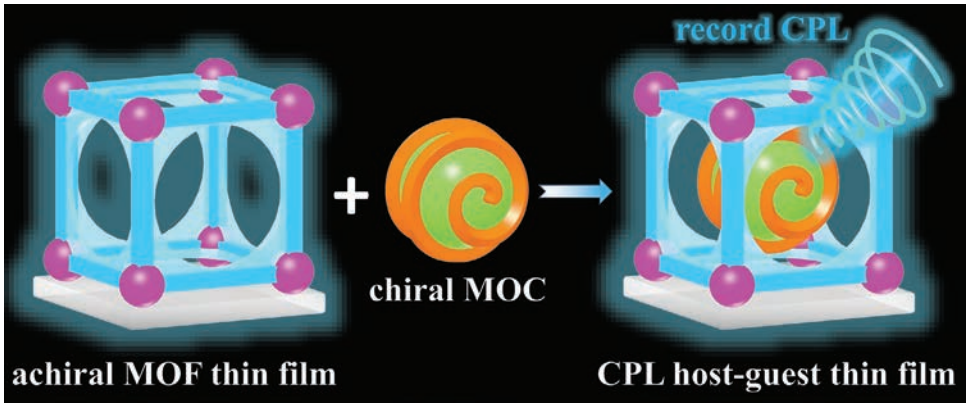

Scheme 1. Schematic diagram of CPL host–guest thin film by loading chiral MOC in achiral MOF for record CPL.

The powder form of MOFs is generally inappropriate for optical applications.[13] High-quality MOF thin film is a prerequisite for the reliable characterization of photophysical properties as well as for device integration.[14] The liquid-phase epitaxy (LPE) layer-by-layer (lbl) procedure is a method particularly well suited for the fabrication of high-quality MOF thin films, yielding so-called SURMOFs (surface-coordinated MOF thin films).[15] Since this method also allows for the epitaxial lbl loading with guest species by the assembly and growth of a layer of metal ions, a layer of ligands, and a layer of guests, this approach has been used here.

The general approach for fabricating efficient CPL material from chiral MOC and achiral fluorescent MOF thin film is depicted in **Scheme 1**. The parent structure is the highly stable photoluminescent zirconium-based MOF NU-901, which contains photoactive-conjugated pyrene-derived linkers and large 3D channels with sizes of 1.57 nm.[16] In this work, the fluorescent, high porous, and oriented NU-901 SURMOF thin film is first prepared using the LPE lbl growth strategy. Enantiopure titanium-organic clusters $Ti_4(OH)_4$(R/S-BINOL)$_6$ (R/S-TOCs, BINOL = 1,1'-bi-2-naphthol) with a size of 1.56 nm were chosen as chiral guests due to their strong chirality, conjugated aggregation, and chemical stability. In addition, as shown in Figure S1 (Supporting information), these R/S-TOCs would fill almost all space available in the NU-901 pores due to their close sizes,[17] which is a prerequisite for obtaining the close contacts to the pyrene linkers required for inducing chirality. Since the large size of these guests prohibits loading via indiffusion, the MOCs were positioned in the pores of NU-901 SURMOF by integrating the loading process into the lbl SURMOF fabrication process. The merit of this approach, which allows loading guests with sizes larger than the MOF channels, has been reported previously.[17,18] The obtained R- and S-TOC@NU-901 SURMOFs exhibit strong cyan emission, similar to the parent NU-901 SURMOFs, but show pronounced clockwise and counter-clockwise circular polarization originating from the chirality induced by the R- and S-TOCs, respectively. The R- and S-TOC@NU-901 SURMOFs have strong CPL signals, with the largest g_{lum} of ± 0.025 reported so far for the downshifted MOF-based CPL material. We attribute this high efficiency to a very good electronic coupling between the achiral, pyrene-derived photoactive linkers in the MOF and the chiral MOCs. This hypothesis is corroborated by density functional theory calculations showing the presence of strong π–π stacking interactions as well as by the comparison to reference systems obtained by loading two similar chiral guests (R/S-BINOL and R/S-1,2-diaminocyclohexane (R/S-DCH)) into the parent NU-901 SURMOFs. This study not only presents novel chiral guest-induced MOF thin film but also provides a new route for designing materials for CPL applications by encapsulating chiral clusters into achiral MOFs.

NU-901 SURMOF was fabricated by using the LPE lbl dipping process[18b,19] as shown in **Figure 1**a. The hydroxyl-functionalized quartz substrate was subsequently immersed into DMF solutions of $ZrCl_4$ with benzoic acid, 1,3,6,8-tetra(4-carboxylphenyl)pyrene (TBAPy), and DMF washing solution to obtain NU-901 SURMOF (Figure S2, Supporting information). Typically, 100 cycles were used (for details see the Supporting Information). The out-of- and in-plane XRD (Figure 1b) patterns showed diffraction peaks at 5.2°, 5.4°, 7.4°, 8.9°, 10.4°, 10.7°, and 15.6°, which can be all indexed in the orthorhombic space group Cmmm (#65). These results are fully consistent with the simulated XRD pattern of the NU-901 structure reported previously by Farha et al.,[16] showing the NU-901 SURMOF had the characteristics of preferred orientation grown along the [110] direction. IR spectra recorded for the NU-901 SURMOF (Figure S3, Supporting information) showed the absence of hydroxyl stretching (2657 cm^{-1}) and carboxyl stretching vibrations (1654 cm^{-1}), indicating the coordination between Zr ions and TBAPy ligands.[20] The surface and cross-sectional SEM images (Figure 1c) of NU-901 SURMOF revealed the presence of compact, monolithic, and homogeneous thin films with thicknesses of ≈200 nm. The photoluminescence spectra (Figure 1d) recorded for NU-901 SURMOF under an excitation wavelength of 400 nm (Figure S4, Supporting information) revealed a strong emission at 500 nm, red-shifted by ≈50 nm relatively compared to that (446 nm) of the solvated TBAPy ligands (Figure S5, Supporting information).

In the next step, R/S-TOCs were loaded into the parent NU-901 MOF using the epitaxial lbl encapsulation strategy (**Figure 2**a). The R/S-TOCs were synthesized by solvothermal reaction of the R/S-BINOL and tetraisopropyl titanate in DMF/isopropanol solutions, as described in previous work.[17] XRD patterns, IR spectra, and UV-vis absorbance spectra (Figures S6–S8, Supporting information) indicated the successful synthesis of R/S-TOCs. The epitaxial lbl encapsulation strategy involved the immersion

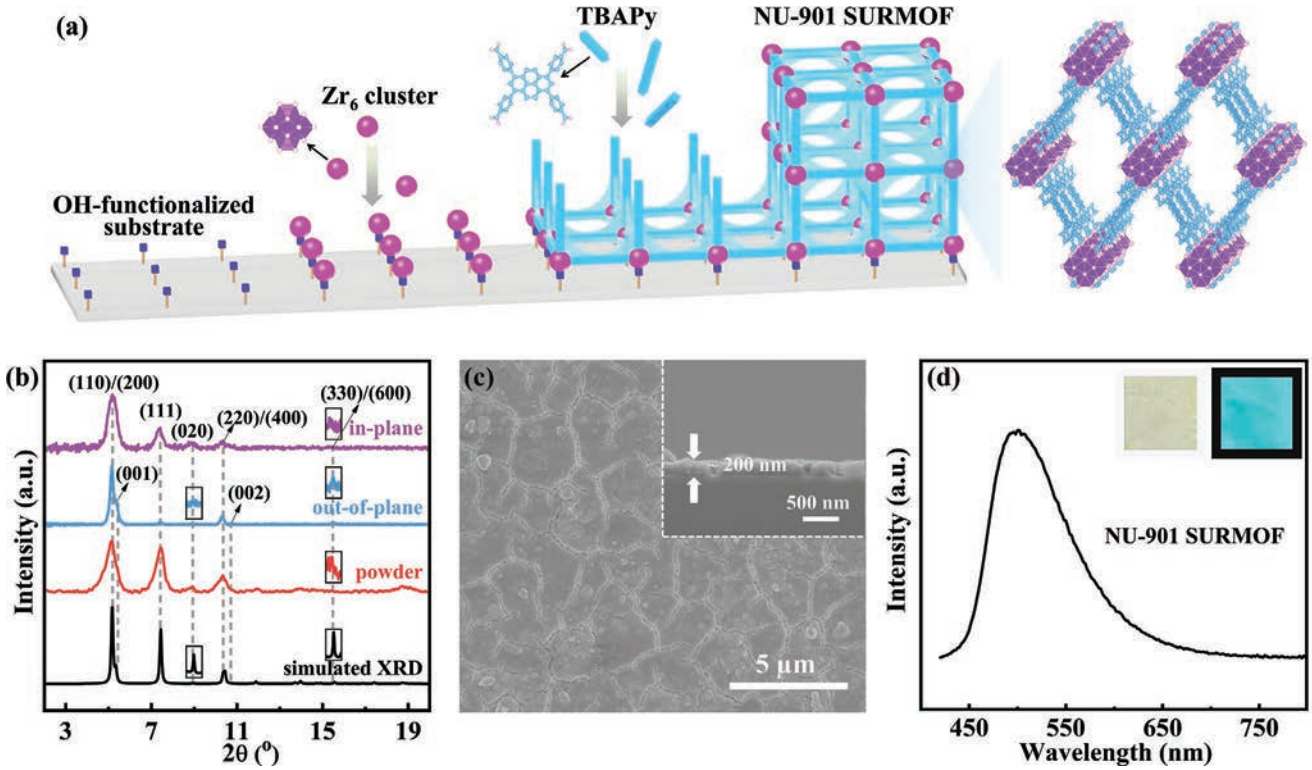

Figure 1. a) Schematic diagram for preparation of NU-901 SURMOF by using LPE lbl method; characterizations of NU-901 SURMOF: b) XRD patterns, c) surface and cross-sectional (inset) SEM morphologies, and d) photoluminescence spectrum and the corresponding photographs under natural light (left, inset) and 365 nm UV-light (right, inset) irradiation.

of the functionalized substrate into the solutions of metal ions, TBAPy ligands, and R-TOC solutions sequentially to obtain R-TOC@NU-901 SURMOF. The XRD patterns (Figure 2b) suggested that the periodic structure of NU-901 was maintained. However, the relative intensities of (220)/(400) and (330)/(600) diffraction peaks are increased relative to the (empty) parent NU-901 SURMOF. This change in the XRD patterns reveals the success in loading TOC guests in virtually all pores of the parent MOF.[17] The presence of the TOC guests was also demonstrated by the IR spectra (Figure S9, Supporting information) of R-TOC@NU-901 SURMOF, which showed bands at 1334, 1236, and 973 cm^{-1} ascribed to carbonyl vibrations of R-TOC. The UV–vis spectra (Figure S10, Supporting information) showed a decreased absorption peak at 321 nm and a slightly increased absorption peak at 367 nm relative to the parent (empty) NU-901 SURMOF, indicating the existence of charge transfer between R-TOC and NU-901.[21] Moreover, the change in porosity upon loading with the TOC was demonstrated by a QCM-based gravimetric detection scheme. As shown in Figure 2c, the ethanol uptake of the pristine NU-901 SURMOF amounted to 5.78 µg cm^{-2}, then decreased to 3.07 µg cm^{-2} after loading with R-TOC, indicating the porosity became smaller due to a part of MOF pores were occupied by the guest. Furthermore, electron spray ionization (ESI) mass spectra (Figure S11, Supporting information) of R-TOC before and after loading in NU-901 SURMOF were found at the range from 1965.31 to 2111.41 m z^{-1}, showing a consistent with the simulated R-TOC with 0–2 DMF molecules. The result demonstrates the chiral TOCs remain intact upon encapsulation into the MOF pores.

Together, these findings provide compelling evidence that the guests were loaded into basically all pores contained in NU-901 MOF. In addition, the surface morphologies (Figure 2d) of R-TOC@NU-901 SURMOF remained unchanged relative to the parent NU-901 SURMOFs. TEM element mapping images (Figure 2e) showed a homogeneous distribution of Zr, C, O, and Ti elements in R-TOC@NU-901, demonstrating that R-TOC was encapsulated in NU-901 homogeneously. Similar results were obtained for the other enantiomer. S-TOC@NU-901 SURMOF was prepared by using the same process, and the successful formation was demonstrated by the XRD patterns, IR spectra, UV–vis spectra, QCM adsorption, SEM, and TEM element mapping images (Figures S10 and S12–16, Supporting information).

Since the guest TOC with the size of 1.56 nm is close to the channel of MOF (1.57 nm) but smaller than the pore of the MOF, a conventional loading via indiffusion initiated by immersion NU-901 into solutions of the TOC is expected to be inefficient. This expectation is confirmed by test experiments, where NU-901 SURMOF was immersed into TOC solutions. The IR and QCM data (Figures S17–S18, Supporting information) showed that there was no indiffusion of TOC into the MOF NU-901. Achieving high loading ratios thus is only possible with the integrated lbl method.

The obtained R- and S-TOC@NU-901 SURMOFs were then subjected to a thorough investigation of their photoluminescence and chirality properties. As shown in **Figure 3**a, the photoluminescence spectra of R- and S-TOC@NU-901 SURMOFs under an excitation wavelength of 400 nm (Figure S19, Supporting

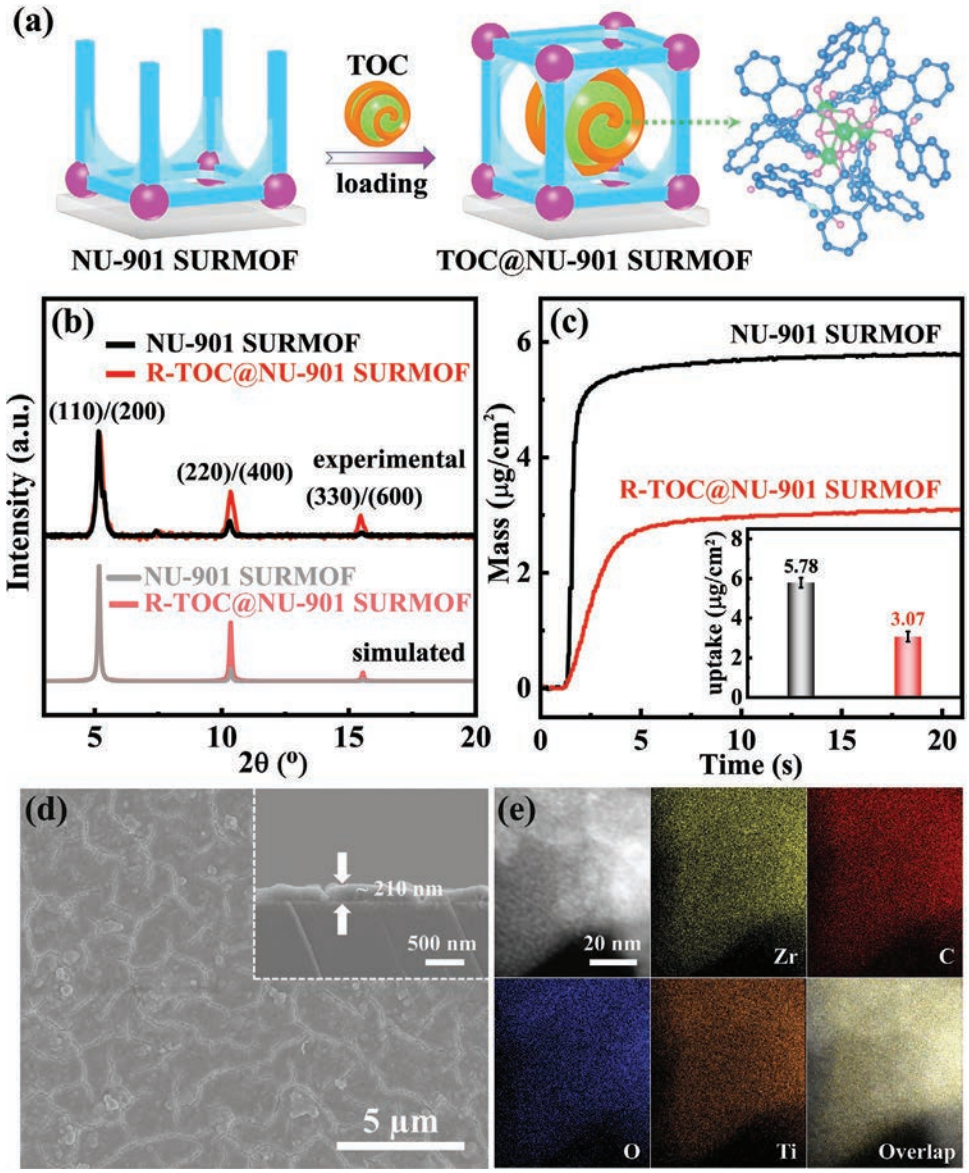

Figure 2. a) Schematic diagram of TOC@NU-901 SURMOF by encapsulating chiral TOCs in photoluminescent NU-901 SURMOF; characterizations of R-TOC@NU-901 SURMOF: (b) XRD patterns, (c) mass uptake with error bars of ethanol by using a gas phase QCM technique, d) surface and cross-sectional (inset) SEM images, and e) TEM element mapping images.

information) exhibited strong emission at 506 nm, only slightly shifted relative to the parent (empty) NU-901 SURMOF. Since the TOCs do not show luminescence in this regime (Figure S20, Supporting information), both adsorption and emission take place within the pyrene-derive linkers of NU-901.

The photoluminescent intensity of NU-901 SURMOF decreased after loading with the TOCs. Together with the small shift in emission frequency, this observation suggests the presence of a host/guest electronic coupling. We feel that a donor/acceptor charge transfer between the TOCs and the pyrene-derived NU-901 linkers is the most likely mechanism.[22] Circular dichroism (CD) data recorded for two reference systems. R/S-TOCs showed pronounced differences from the R/S-BINOL (Figure S21, Supporting information). The CD spectra (Figure 3b) recorded for R-TOC@NU-901 SURMOF exhibited two positive bands at 270 and 340 nm, and one negative band at 370 nm, which are very similar to those obtained for solvated R-TOC. The enantiomeric S-TOC@NU-901 SURMOF showed CD bands of about the same size but opposite signals compared to R-TOC@NU-901, as expected.

Although the position of the emission bands is dictated by the pyrene linkers, the chiral signal is induced by the chiral guests. This is confirmed by Figure S22 (Supporting information), which demonstrates that there is no chiral property for the parent (empty) MOF. Besides, we found that the UV–vis absorption of R/S-TOC@NU-901 SURMOFs at 268 nm increased compared with the pristine NU-901 SURMOF, and the ratio of intensity at 268 nm versus 335 nm in the

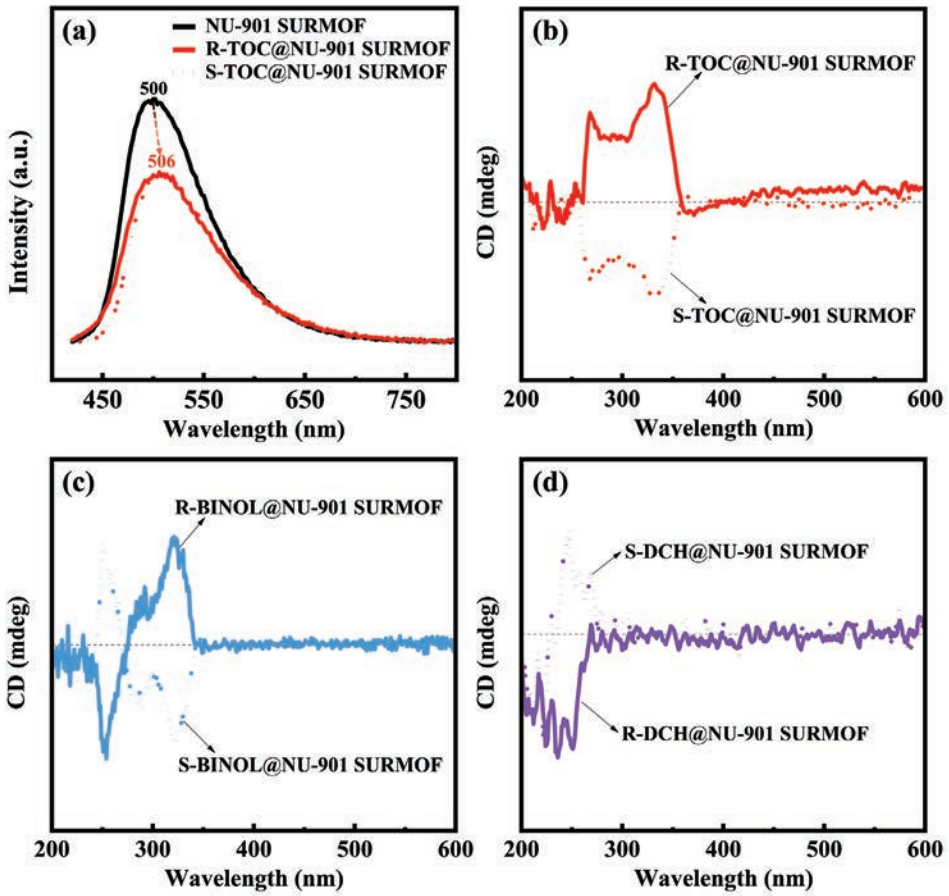

Figure 3. a) Photoluminescence spectra of NU-901 and R- and S-TOC@NU-901 SURMOFs under the excitation wavelength of 400 nm; b) CD spectra of R- and S-TOC@NU-901, c) R- and S-BINOL@NU-901, and d) R- and S-DCH@NU-901 SURMOFs.

corresponding CD spectrum was also enhanced after encapsulating R/S-TOC (Figure S23, Supporting information), which may be because the interaction between R/S-TOC and NU-901 results in the chirality of TOC transfer to NU-901.[23]

To demonstrate that the observed chiral inductions are specific to the strong interaction between the TOCs and pyrene-derived linkers, two other chiral guests that are a component of the TOCs (namely R/S-BINOL) and R/S-DCH were loaded into the NU-901 SURMOFs. The latter compound has no conjugated system. Using the same synthesis conditions, the number of growth layers and molar amount of loading as those used for the R/S-TOCs, well-defined R-, and S-BINOL@NU-901, as well as R- and S-DCH@NU-901 SURMOFs could be prepared (for characterization details see Supporting Information). Wherein, the mass percentages of C, O, and N elements in R-TOC@NU-901, R-BINOL@NU-901, and R-DCH@NU-901 by the elemental analyzer were shown in Table S2 (Supporting information), and we calculated that the molar ratio of R-TOC and NU-901 was 1.03:1.63 in R-TOC@NU-901, R-BINOL and NU-901 was 7.24:1.61 in R-BINOL@NU-901, and R-DCH and NU-901 was 16.68:1.75 in R-DCH@NU-901. In addition, due to the layer-by-layer encapsulation strategy being a saturated loading process,[24] it is difficult to control the same amounts of loading. QCM data (Figure S24, Supporting information) proved the samples were successfully prepared due to the decreased ethanol uptake compared with the pristine SURMOF. Besides, the small chiral guest BINOL is difficult to load into R-TOC@NU-901 observed by the QCM and IR data (Figures S25–S26, Supporting information). The CD spectra (Figure 3c,d) of R- and S-BINOL@NU-901, and R- and S-DCH@NU-901 SURMOFs showed the clear CD signals derived from the corresponding chiral guests (Figures S27 and S28, Supporting information). Similarly, the relative intensity ratio of CD spectra (Figure S27, Supporting information) of the peak position at 252 nm of R/S-BINOL@NU-901 SURMOFs is much higher than that (266 nm) of R/S-BINOL, also indicating the chirality transfer from the chiral guest to MOF. However, the CD signal of R/S-DCH@NU-901 SURMOFs has only a band, showing that there is almost no obvious chirality transfer. Moreover, all the samples also showed photoluminescent properties originating from the fluorescent host (Figures S29–S30, Supporting information).

In addition, the photoluminescence lifetime decay curves are shown in **Figure 4**a, and the related lifetime parameters with quantum yields (QY) are listed in Tables S3 and S4 (Supporting information). The lifetimes of the sample were fitted by bi-exponential function, indicating the average lifetimes of R-TOC@NU-901 SURMOF (1.33 ns) and S-TOC@NU-901 SURMOF (1.43 ns) were shorter than that of NU-901 SURMOF (1.87 ns). The decreased decay time reveals the energy transfer from NU-901 to TOC.

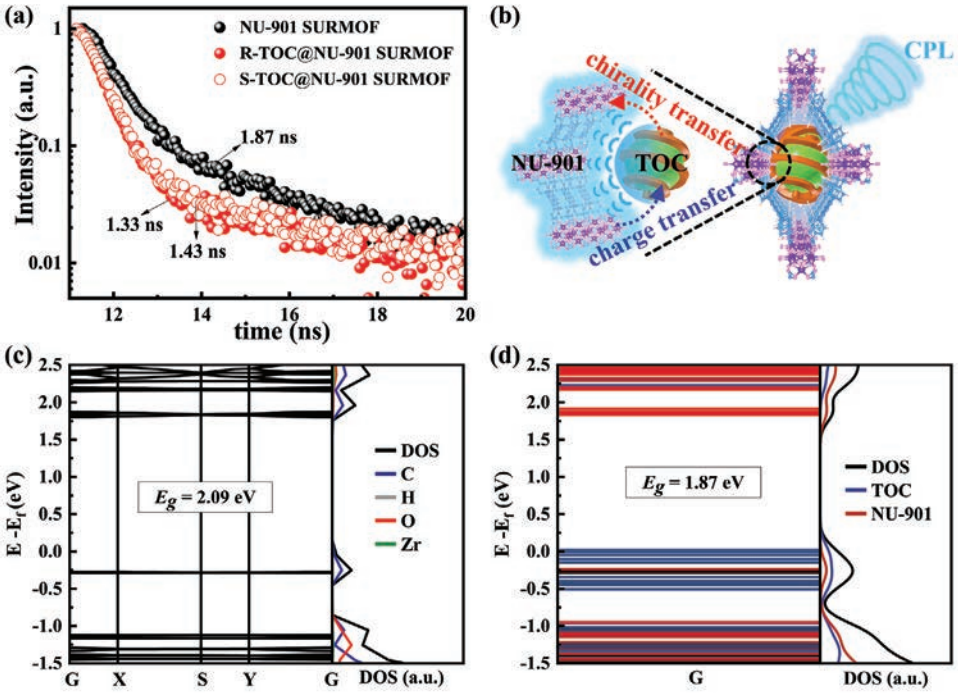

Figure 4. a) Photoluminescence lifetime decay curves of NU-901, R- and S-TOC@NU-901 SURMOFs; b) schematic illustration of the possible charge and chirality transfers produced in TOC@NU-901 for the induction of CPL; electronic band structures and density of states (DOS) of c) NU-901 and d) TOC@NU-901 SURMOFs.

However, the fluorescent lifetimes of powder NU-901 physically mixed with TOCs were no significant difference (Figure S31 and Table S5, Supporting information), implying energy transfer between the donor and acceptor[25] only occurred in the host–guest system. Interestingly, the photocurrent curves (Figure S32, Supporting information) showed the host–guest thin films after encapsulating the guests (R-TOC, R-BINOL, and R-DCH) have better photosensitivity compared to the pristine NU-901 SURMOF, in which R-TOC@NU-901 has the best photosensitivity. It suggested that loading R-TOC in NU-901 SURMOF would effectively suppress the recombination of electron-hole pairs and would transfer more electrons, which further illustrates that the interaction between the guest and host MOF can promote the charge transfer. Moreover, the ultrafast time-resolved transient absorption (TA) spectroscopy was performed with the delays following the excitation by a 400 nm pump pulse. The TA spectra (Figure S33, Supporting information) of NU-901 SURMOF and after encapsulating the three chiral guests probed under different delay times had a broad-band excited state absorption feature ($\Delta A > 0$) centered at ≈600 nm. It indicated that the electrons of host NU-901 SURMOF in the excited state would absorb light and transfer to a higher excited state. After loading the chiral guests (R-TOC, R-BINOL, and R-DCH), the interaction between the NU-901 and guests would promote more electrons transfer to the higher excited state,[26] showing a much stronger excited state absorption feature. Wherein, the R-TOC@NU-901 demonstrated the maximum ΔA due to the strongest interaction between the guest and host for charge transfer. The representative diagrams (Figures 4b; Figure S34, Supporting information) of TOC@NU-901 SURMOF, TOC mixed NU-901 powder, BINOL@NU-901, and DCH@NU-901 SURMOFs exhibited that the charge and chirality transfers caused by the abundant π–π interactions between TOC and NU-901. As a result, R- and S-TOC@NU-901 SURMOFs exhibited excellent CPL performance due to the special combination of host–guest interaction.

To further illustrate the role of encapsulated TOC in NU-901, density functional theory (DFT) calculations were performed with the structural unit cell as the calculation model, and the calculated path of primitive orthorhombic and atomistic representations of the TOC, NU-901, and TOC@NU-901 along with different crystallographic directions as shown in Figures S35–S36 (Supporting information). The electronic band structure demonstrated NU-901 with a direct bandgap of 2.09 eV, and the density of state (DOS) revealed that states in MOF were dominated by C and O atoms (Figure 4c). As shown in Figure 4d, after encapsulating TOC in the nanopores of NU-901, TOC@NU-901 showed a narrower bandgap of 1.87 eV compared with the pristine MOF, and the DOS of TOC@NU-901 proved that TOC played an important role in the system. Moreover, the optimized structure configuration and the calculated binding energy [E_{BE} = E(TOC@NU-901)-E(TOC)-E(NU-901)] of –1.15 eV indicated that there is an obvious interaction between TOC and NU-901.

The CPL reflects chiral fluorescent information about the excited state.[27] A quantitative measure of CPL is the g_{lum} value, defined as $g_{lum} = 2 \times (I_L - I_R)/(I_L + I_R)$ (where I_L and I_R are the intensities of left- and right-handed CPL, respectively). Due to the anisotropy of the thin film sample in the CPL measurement, we obtained multiple values by rotating each sample every

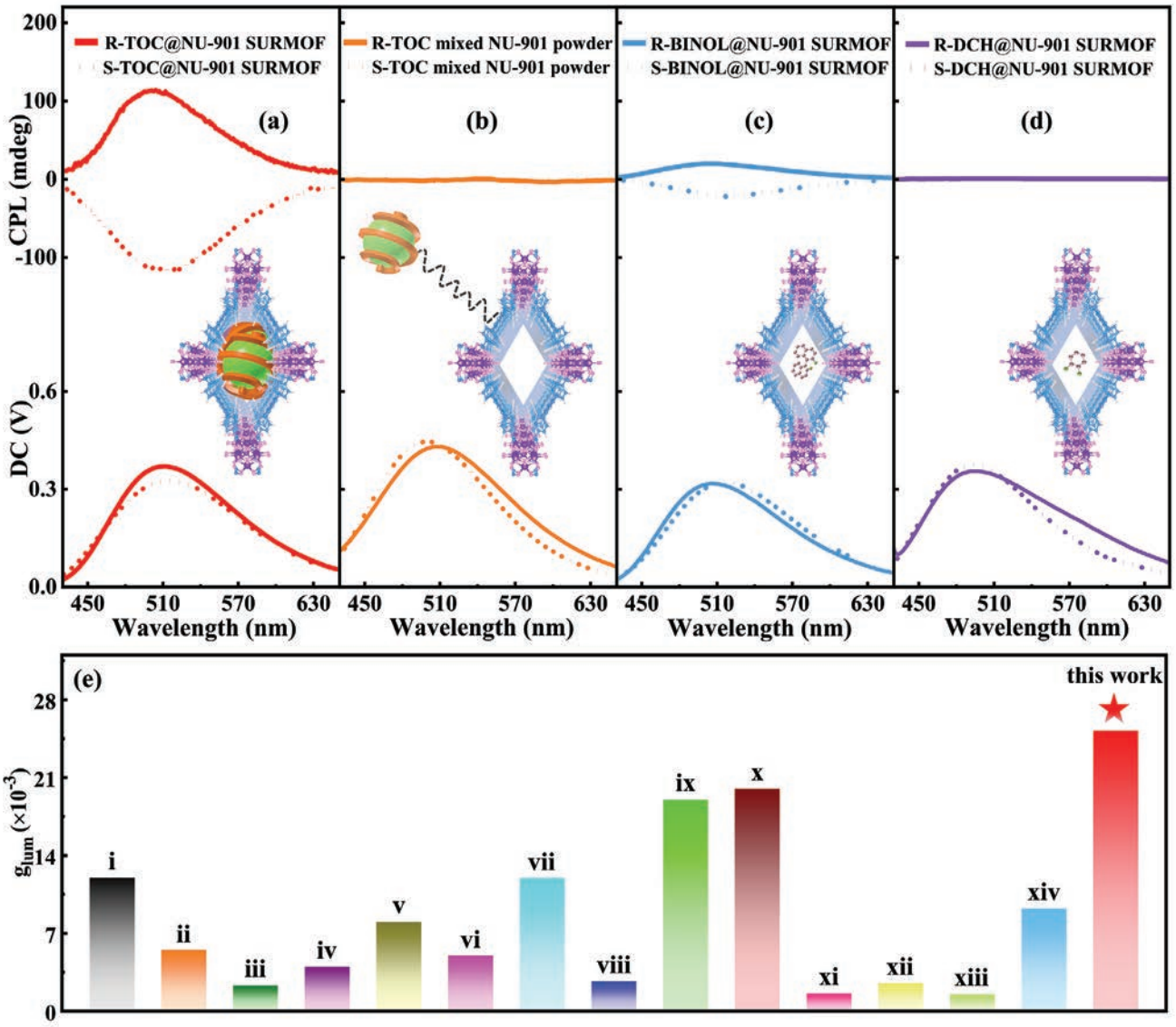

Figure 5. CPL spectra: a) R- and S-TOC@NU-901 SURMOFs, b) R- and S-TOC mixed NU-901 powder, c) R- and S-BINOL@NU-901 SURMOFs, and d) R- and S-DCH@NU-901 SURMOFs. e) Comparison of g_{lum} value of TOC@NU-901 SURMOFs with the reported downshifted MOF-based materials: i AIEgen MOF;[7a] ii chiral ZIFs;[7b] iii eta MOFs;[7c] iv $[Ln_2(\mu_4\text{-tar})_2(\mu\text{-tar})(H_2O)_2]\cdot xH_2O$;[7d] v $Zn_2(D/LCam)_2DAP$;[7e] vi ZIF-8;[8a] vii $Zn(l/d\text{-}l_{Cl})(Cl)](H_2O)_2$;[11a] viii MOF-1;[11b] ix γCD-MOF;[11c] x LaTCPB;[11d] xi $Eu(BTC)(H_2O)$;[11e] xii TbBTC;[11f] xiii $[Ag_{12}(S^tBu)_6(CF_3CO_2)_6(tppe)_{1.5}](DMAC)_{39}$;[11g] xiv $[Zn_2(D/Lcam)_2dabco]_n$.[11h]

60° and averaging it. The two-handedness CPL signals of R- and S-TOC@NU-901 SURMOFs are shown in Figure S37 (Supporting information), and the corresponding average values are displayed in **Figure 5**a. The results reveal strong CPL signals, with the opposite sign for the two enantiomeric host–guest thin films. The corresponding maximal g_{lum} values (Figure S38, Supporting information) for R- and S-TOC@NU-901 SURMOFs reached ± 0.025. Reference samples fabricated using 1:1 mixtures of NU-901 and R- or S-TOCs powder showed no CPL signal (Figure 5b).

Further, the CPL signals recorded for the R/S-BINOL reference systems (Figures 5c (corresponding average values); Figure S39, Supporting information) were much weaker, with maximal g_{lum} values of ± 0.005 (Figure S40, Supporting information), almost one order of magnitude smaller than for TOC@NU-901 SURMOFs. Notably, R- and S-DCH@NU-901 SURMOFs showed no CPL performance at all (Figure 5d; Figure S41, Supporting information). This comparison reveals that an achiral, luminescent MOF by simply loading with a chiral guest is not sufficient for the induction of circular polarization, yielding circularly polarized emission that requires a strong electronic coupling to the chromophoric components of the host MOF. Interestingly, compared to the reported downshifted MOF-based CPL materials (Figure 5e and Table S1, Supporting information), it is the first preparation of guest-induced host–guest CPL thin films by encapsulating chiral MOCs into achiral MOF thin film and achieves an excellent CPL performance with the highest g_{lum}.

2. Conclusions

In summary, we have designed and fabricated a new type of guest-induced CPL material by encapsulating chiral MOCs into achiral photoluminescent MOF thin film. A highly stable, zirconium pyrene-based NU-901 SURMOF with intense photoluminescent emission was first prepared by using the LPE lbl method and served as a host matrix. A pair of enantiomers R- and S-TOCs was loaded into the nanopores of NU-901 SURMOF to form host–guest R- and S-TOC@NU-901 SURMOFs for studying chiroptical properties. The photoluminescence and CD spectra recorded for R- and S-TOC@NU-901 SURMOFs exhibited strong photoluminescent emission at ≈500 nm and obvious chiral signals with excellent CPL performance. The g_{lum}-factor amounted to ± 0.025 and was much higher than that observed for other chiral guests, R- and S-BINOL@NU-901, R- and S-DCH embedded in the same MOF as well as for other downshifted MOF-based CPL materials. The excellent performance of the TOC@NU-901 SURMOFs can be related to an effective chiral induction and charge transfer brought about by the close contact of the embedded chiral conjugated centers and the chromophoric MOF linkers. Most importantly, the large size of the guests prohibited loading via indiffusion and required the use of an integrated layer-by-layer strategy. This proof-of-principle work provides a novel avenue toward MOF-based CPL applications, in particular concerning circularly polarized electroluminescent devices.

Supporting Information

Supporting Information is available from the Wiley Online Library or from the author.

Acknowledgements

This work was supported by the National Natural Science Foundation of China (21872148), the Youth Innovation Promotion Association of the Chinese Academy of Sciences (2018339), and Fujian Science & Technology Innovation Laboratory for Optoelectronic Information of China (Grant No. 2021ZR131). C.W. acknowledges support from Deutsche Forschungsgemeinschaft (DFG, German Research Foundation) under Germany's Excellence Strategy—2082/1—390761711.

Conflict of Interest

The authors declare no conflict of interest.

Data Availability Statement

The data that support the findings of this study are available in the supplementary material of this article.

Keywords

circularly polarized luminescence, host–guest interactions, metal–organic frameworks, thin films

[1] a) M. H. Liu, L. Zhang, T. Y. Wang, *Chem. Rev.* **2015**, *115*, 7304; b) M. Hu, H. T. Feng, Y. X. Yuan, Y. S. Zheng, B. Z. Tang, *Coord. Chem. Rev.* **2020**, *416*, 213329; c) J. M. Han, S. Guo, H. Lu, S. J. Liu, Q. Zhao, W. Huang, *Adv. Opt. Mater.* **2018**, *6*, 1800538.
[2] T. Ikai, M. Okubo, Y. Wada, *J. Am. Chem. Soc.* **2020**, *142*, 3254.
[3] Y. X. Yuan, M. Hu, K. R. Zhang, T. T. Zhou, S. Wang, M. H. Liu, Y. S. Zheng, *Mater. Horiz.* **2020**, *7*, 3209.
[4] a) D. Niu, Y. Jiang, L. Ji, G. Ouyang, M. Liu, *Angew. Chem., Int. Ed.* **2019**, *58*, 5946; b) Y. Zhu, J. Guo, X. Qiu, S. Zhao, Z. Tang, *Accounts Mater. Res.* **2021**, *2*, 21.
[5] J. Zhao, T. J. Zhang, X. Y. Dong, M. E. Sun, C. Zhang, X. L. Li, Y. S. Zhao, S. Q. Zang, *J. Am. Chem. Soc.* **2019**, *141*, 15755.
[6] J. R. Long, O. M. Yaghi, *Chem. Soc. Rev.* **2009**, *38*, 1213.
[7] a) W. L. Shang, X. F. Zhu, T. L. Liang, C. Du, L. Y. Hu, T. S. Li, M. H. Liu, *Angew. Chem., Int. Ed.* **2020**, *59*, 12811; b) T. H. Zhao, J. L. Han, X. Jin, Y. Liu, M. H. Liu, P. F. Duan, *Angew. Chem., Int. Ed.* **2019**, *58*, 4978; c) X. Z. Wang, M. Y. Sun, Z. J. Huang, M. Xie, R. S. Huang, H. H. Lu, Z. J. Zhao, X. P. Zhou, D. Li, *Adv. Opt. Mater.* **2021**, *9*, 2002096; d) U. Huizi-Rayo, A. Zabala-Lekuona, A. Terenzi, C. M. Cruz, J. M. Cuerva, A. Rodríguez-Diéguez, J. A. García, J. M. Seco, E. San Sebastian, J. Cepeda, *J. Mater. Chem. C* **2020**, *8*, 8243; e) S. M. Chen, L. M. Chang, X. K. Yang, T. Luo, H. Xu, Z. G. Gu, J. Zhang, *ACS Appl. Mater. Interfaces* **2019**, *11*, 31421.
[8] a) T. Zhao, J. Han, X. Jin, M. Zhou, Y. Liu, P. Duan, M. Liu, *Research* **2020**, *2020*, 6452123; b) M. N. Huang, R. N. Yu, K. Xu, S. X. Ye, S. Kuang, X. H. Zhu, Y. Q. Wan, *Chem. Sci.* **2016**, *7*, 4485.
[9] a) L. Y. Chen, Q. Xu, *Matter* **2019**, *1*, 57; b) M. Y. Masoomi, A. Morsali, A. Dhakshinamoorthy, H. Garcia, *Angew. Chem., Int. Ed.* **2019**, *58*, 15188; c) X. Z. Lian, Y. Fang, E. Joseph, Q. Wang, J. L. Li, S. Banerjee, C. Lollar, X. Wang, H. C. Zhou, *Chem. Soc. Rev.* **2017**, *46*, 3386; d) J. Aguilera-Sigalat, D. Bradshaw, *Coord. Chem. Rev.* **2016**, *307*, 267; e) J. Perego, C. Bezuidenhout, I. Villa, F. Cova, R. Crapanzano, I. Frank, F. Pagano, N. Kratochwill, E. Auffray, S. Bracco, *ChemRxiv*, **2021**, preprint, https://doi.org/10.26434/chemrxiv-2021-j78m4.
[10] a) H. Y. Zhang, B. L. Wang, X. W. Yu, J. Y. Li, J. Shang, J. H. Yu, *Angew. Chem., Int. Ed.* **2020**, *59*, 19390; b) Y. T. Sang, J. L. Han, T. H. Zhao, P. F. Duan, M. H. Liu, *Adv. Mater.* **2020**, *32*, 1900110.
[11] a) C. Zhang, Z. P. Yan, X. Y. Dong, Z. Han, S. Li, T. Fu, Y. Y. Zhu, Y. X. Zheng, Y. Y. Niu, S. Q. Zang, *Adv. Mater.* **2020**, *32*, 2002914; b) H. R. Fu, N. Wang, X. X. Wu, F. F. Li, Y. Zhao, L. F. Ma, M. Du, *Adv. Opt. Mater.* **2020**, *8*, 2000330; c) L. Y. Hu, K. Li, W. L. Shang, X. F. Zhu, M. H. Liu, *Angew. Chem., Int. Ed.* **2020**, *59*, 4953; d) T. H. Zhao, J. L. Han, Y. H. Shi, J. Zhou, P. F. Duan, *Adv. Mater.* **2021**, *33*, 2101797; e) C. Zhang, Z. S. Li, X. Y. Dong, Y. Y. Niu, S. Q. Zang, *Adv. Mater.* **2022**, *34*, 2109496; f) M. Zeng, A. Ren, W. B. Wu, Y. S. Zhao, C. L. Zhan, J. N. Yao, *Chem. Sci.* **2020**, *11*, 9154; g) X.-H. Wu, Z. Wei, B.-J. Yan, R.-W. Huang, Y.-Y. Liu, K. Li, S.-Q. Zang, T. C. W. Mak, *CCS Chem* **2019**, *1*, 553; h) R. Zhai, Y. H. Xiao, Z. G. Gu, J. Zhang, *Nano Res.* **2022**, *15*, 1102.
[12] a) F. de Azambuja, J. Moons, T. N. Parac-Vogt, *Accounts Chem. Res.* **2021**, *54*, 1673; b) Z. Lei, X. L. Pei, Z. J. Guan, Q. M. Wang, *Angew. Chem., Int. Ed.* **2017**, *56*, 7117; c) G. C. Deng, B. K. Teo, N. F. Zheng, *J. Am. Chem. Soc.* **2021**, *143*, 10214.
[13] R. Haldar, L. Heinke, C. Wöll, *Adv. Mater.* **2020**, *32*, 1905227.
[14] a) O. Shekhah, J. Liu, R. A. Fischer, C. Wöll, *Chem. Soc. Rev.* **2011**, *40*, 1081; b) S. Okur, P. Qin, A. Chandresh, C. Li, Z. J. Zhang, U. Lemmer, L. Heinke, *Angew. Chem., Int. Ed.* **2020**, *60*, 3566; c) J. X. Wang, J. Yin, O. Shekhah, O. M. Bakr, M. Eddaoudi, O. F. Mohammed, *ACS Appl. Mater. Interfaces* **2022**, *14*, 9970.
[15] Y. H. Xiao, Z. G. Gu, J. Zhang, *Nanoscale* **2020**, *12*, 12712.
[16] L. Robison, R. J. Drout, L. R. Redfern, F. A. Son, M. C. Wasson, S. Goswami, Z. Chen, A. Olszewski, K. B. Idrees, T. Islamoglu, O. K. Farha, *Chem. Mater.* **2020**, *32*, 3545.
[17] Z. G. Gu, H. Fu, T. Neumann, Z. X. Xu, W. Q. Fu, W. Wenzel, L. Zhang, J. Zhang, C. Wöll, *ACS Nano* **2016**, *10*, 977.

[18] a) X. J. Liu, M. Kozlowska, T. Okkali, D. Wagner, T. Higashino, G. Brenner-Weifss, S. M. Marschner, Z. H. Fu, Q. Zhang, H. Imahori, S. Brase, W. Wenzel, C. Wöll, L. Heinke, *Angew. Chem., Int. Ed.* **2019**, *58*, 9590; b) D. J. Li, Z. G. Gu, J. Zhang, *Chem. Sci.* **2020**, *11*, 1935.
[19] Z. G. Gu, A. Pfriem, S. Hamsch, H. Breitwieser, J. Wohlgemuth, L. Heinke, H. Gliemann, C. Wöll, *Micropor. Mesopor. Mat.* **2015**, *211*, 82.
[20] B. Zhao, Q. Yang, J. S. Wang, F. Y. Xie, H. Y. Yu, Y. Li, Y. X. Ma, W. J. Ruan, *New J. Chem.* **2021**, *45*, 4401.
[21] S. Goswami, D. Ray, K. Otake, C. W. Kung, S. J. Garibay, T. Islamoglu, A. Atilgan, Y. X. Cui, C. J. Cramer, O. K. Farha, J. T. Hupp, *Chem. Sci.* **2018**, *9*, 4477.
[22] a) C. W. Kung, K. Otake, C. T. Buru, S. Goswami, Y. X. Cui, J. T. Hupp, A. M. Spokoyny, O. K. Farha, *J. Am. Chem. Soc.* **2018**, *140*, 3871; b) J. Perego, I. Villa, A. Pedrini, E. C. Padovani, R. Crapanzano, A. Vedda, C. Dujardin, C. X. Bezuidenhout, S. Bracco, P. E. Sozzani, A. Comotti, L. Gironi, M. Beretta, M. Salomoni, N. Kratochwil, S. Gundacker, E. Auffray, F. Meinardi, A. Monguzzi, *Nat. Photonics* **2021**, *15*, 393.
[23] D. Yang, P. F. Duan, L. Zhang, M. H. Liu, *Nat. Commun.* **2017**, *8*, 15727.
[24] Z. G. Gu, J. Zhang, *Coord. Chem. Rev.* **2019**, *378*, 513.
[25] a) R. Marin, L. Labrador-Paez, A. Skripka, P. Haro-Gonzalez, A. Benayas, P. Canton, D. Jaque, F. Vetrone, *ACS Photonics* **2018**, *5*, 2261; b) K. C. Park, C. Seo, G. Gupta, J. Kim, C. Y. Lee, *ACS Appl. Mater. Interfaces* **2017**, *9*, 38670; c) J. X. Wang, L. Gutierrez-Arzaluz, X. J. Wang, M. Almalki, J. Yin, J. Czaban-Jozwiak, O. Shekhah, Y. H. Zhang, O. M. Bakr, M. Eddaoudi, O. F. Mohammed, *Matter* **2022**, *5*, 253.
[26] J. R. Yu, J. Park, A. Van Wyk, G. Rumbles, P. Deria, *J. Am. Chem. Soc.* **2018**, *140*, 10488.
[27] C. T. Yeung, K. H. Yim, H. Y. Wong, R. Pal, W. S. Lo, S. C. Yan, M. Y. M. Wong, D. Yufit, D. E. Smiles, L. J. McCormick, S. J. Teat, D. K. Shuh, W. T. Wong, G. L. Law, *Nat. Commun.* **2017**, *8*, 42.